université
PARIS-SACLAY

Faculty of Sciences

Quarmen Erasmus Mundus Joint Master

Internship Report

QUANTUM COMPUTING WITH COLD NEUTRAL ATOMS AND LASER ANALYSIS IN PASQAL

Presented by:
David Jesús Árbol Guerrero

Academic year 2023-2024

Summary

This is a report of the different tasks that I, David Jesús Árbol Guerrero, carried out as an intern in Pasqal's System Performance team from 3^{rd} June to 31^{st} July 2024. Pasqal is a quantum computing company that developes *quantum processor units* (QPU) based in ^{87}Rb *cold neutral atoms*. The focus of my internship was within the System Performance Team, which plays a critical role in monitoring, calibrating, and characterizing quantum hardware. The team's primary objective is to ensure the optimal functioning of the quantum system, essential for the accurate manipulation of cold neutral atoms.

Firstly, I worked on documentation work about the operating procedures of the QPUs in Pasqal: *Fresnel 1* and *Fresnel 2*. I summarized the quantum hardware that is used, some specifications and how it works in general. I also explained 4 procedures to characterize some parameters of the optical traps. In the meantime, I attended meetings of the *Fresnel 1* team each Thursday to be aware of the topics that my team was involved in and in parallel, I tried to implement a solution on my own to one of them: I modeled the behavior of an atom in an optical trap while a protocol was performed on the trapping lasers to measure the atom's oscillation frequency.

Secondly, I studied the theoretical model of the 2-level system that Pasqal uses as a qubit. I followed an article that presented a 3-level system composed by a $^{8}7Rb$ and two lasers that can be regarded as a 2-level system. The article presented the results along with some approximations. I have calculated the results myself and detailed the steps to achieve them.

After that, I started with the main topic of my internship. It consisted of calibrating a new acquisition device in charge of measuring the pulsed laser signals that excited the atoms. The signals used for calibrating are square pulses so they are associated to a precise Rabi frequency. Pasqal has a program to create Rabi oscillations with different Rabi frequencies in each run. This is the input, namely, different laser powers. As output, we measure the pulse signal that is sent and the probability of finding the atom in the ground state. My main task is to measure Rabi oscillations, compare the measured Rabi frequencies Ω_{meas} with the input ones Ω_{input} and the voltage acquired with the new acquisition device V_{PD} and obtain the relations $V_{meas} = f(\Omega_{set})$, $\Omega_{real} = g(\Omega_{input})$ and $\Omega_{meas} = h(V_{meas})$. To achieve this I had to program functions in python to characterise the signal. In the end, I could only obtain the relation $V_{meas} = f(\Omega_{set})$ (quadratic dependence) since there was no programs to perform many Rabi frequency measurements at once with the required resolution and due to lack of time.

Finally, as there were anomalies on the square pulses, a colleague asked me to focus on characterizing them. The square pulses presented oscillations on the plateau that varied quadratically with the laser frequency. Moreover, the plateau voltage (pulse power) also varied quadratically with the laser frequency and studied the causes of these issues.

Contents

1 Introduction

Quantum computing represents a revolutionary advancement in computational technology, leveraging the principles of quantum mechanics to process information in fundamentally new ways. At the forefront of this field, the manipulation of cold neutral atoms has emerged as a promising approach for building quantum computers. Cold neutral atoms offer long coherence times and precise control, making them ideal candidates for quantum computation.

2 Cold neutral atom QPUs

In this section I summarize what I learned during my documentation work regarding how a *quantum processor unit* (QPU) works. It is divided in 4 subsections discussing general knowledge about *cold neutral atoms* qubits, general aspects about Pasqal QPUs parts and how they operates, support functions and protocols to characterize the optical traps. The information in this section comes from [1] and summaries by Pasqal about the QPU setup.

2.1 General knowledge: cold neutral atom based qubits

A **qubit based in cold neutral atoms** is a two-level system composed by 2 energy levels of a neutral atom that is cooled and confined in an optical trap. Naturally, the atom has many different energy levels but it can be manipulated using correctly tuned lasers in a way that we can compute unitary transformations that only involve these two levels. We can make 2 or more atoms interact using several lasers that act over them. In the mathematical language, this means computing unitary transformations over the quantum states, that are in the tensor product of Hilbert spaces of the single qubits. To achieve this, the atoms are set in an array (1D, 2D or 3D), also called *layout*, using optical traps (separated by $\sim \mu m$ so that they do not feel one each other). Qualitatively, this is what quantum computing with cold neutral atoms means.

Some of the main **properties** and **advantages** that make this kind of qubit so appealing are:

- **Identical and perfect qubits:** There is no possibility of failure when engineering the qubit as it comes from nature and all of them will have the same properties.
- **High connectivity and scalability:** To perform a quantum gate we need two or more atoms to interact. We can easily make two atoms that are far away interact by moving them closer with optical tweezers. Moreover, we only need to increase the number of moving tweezers and traps to scale the QPU up, and still the quantum system will remain small ($\sim \mu m$).
- **Native multiple qubit gates:** It is possible to natively implement a gate of more than 2 qubits. For example, a Toffoli gate (3 qubit CCNOT gate) is computed by only 7 light pulses.
- **Large lifetime and natural quantum memory:** Using appropiate atoms, the qubits have a large lifetime (order of seconds), what lets us perform a large quantity of quantum gates. Also, there is no need of developing new quantum hardware to be used as a quantum memory because you can move aside the atoms (qubits) that you want to save since they already have a long lifetime.
- **Low energy consumption:** It is one of the qubits that consumes less energy because we only need to cool the atoms down, not a bulk of matter as in the case of superconducting qubits. This is done with an affordable and widely researched method, **laser cooling**.
- **Laser manipulation:** This make them easy to handle in comparison with other technologies.
- **Alkali atoms:** Alkali atoms are perfect for this task. They have long-lived hyperfine levels in the internal ground state, what results in long coherence times. We can use many different possible 2-level systems using hyperfine levels. Rydberg states are excited states with exaggerated properties that ease atom-atom and light-atom interactions so these are perfect to perform the role of $|1\rangle$. After the computation, the atoms can be targeted with

laser light capable of providing enough energy to take the atom out of the trap if it is in the excited state. Therefore, presence or absence of an atom means reading $|0\rangle$ or $|1\rangle$ respectively.

What is more, you can take advantage of the **Rydberg Blockade** property to perform multiple qubits quantum gates and put several atoms into superposition states. In short, two atoms in the ground state $|g\rangle$ that are close enough cannot both promote to the rydberg state $|r\rangle$ when the pair is excited with a laser pulse. Then, with a $\pi - pulse$ the pair can transition from $|gg\rangle$ to $1/\sqrt{2}(|ge\rangle + |eg\rangle)$.

On the other hand, some **drawbacks** are:

- **Long initial state preparation:** Filling all the traps in the array is very unlikely unless we use a protocol with moving optical tweezers, what involves large preparation times.
- **Long moving times and quantum gates:** The long connectivity comes from the ability to move the atoms but moving atoms carries long times.

There are 2 possible **control modes** for this QPU technology:

- **Analogue control:** The evolution of the atoms is given by the Hamiltonian of the atomic system. The user can then manipulate it by using different *layouts* and, therefore, the system is allowed to evolve independently. This is a resource to perform **quantum simulation**, through which the Hamiltonian is tuned to model other quantum system whose behaviour we want to study. One of the main applications is for *drug design* and *material science*.
- **Digital control:** The evolution of the qubits are controled by lasers that performs quantum gates. It is mainly used for *optimisation problems* or *machine learning*.

2.2 Pasqal's QPUs

In this section we present the devices that compose a QPU in Pasqal. They are divided according to on their function. The **main parts of the QPU** are presented hereunder:

- **Register actuators:** Hardware in charge of initializing the quantum register, this is, the initial quantum state of the system (usually $|0...0\rangle$). It includes the laser cooling system, optical traps and tweezers hardware, and the electronics to monitor the process. It is reconstructed after each computation.
- **Processing actuators:** Hardware that performs quantum computation. It implies using laser pulses and electronics to control and monitor them.
- **Quantum register:** Devices that register quantum data results. They collect fluorescence light coming from the atoms that did not escape from its trap (the ones in the ground state). Then, bright means $|0\rangle$ and dark means $|1\rangle$.

We will see now in more detail how these goals are achieved and which devices are used.

2.2.1 Register actuators:

A thin layer of pure ^{87}Rb is heated up inside a ultra high vacuum (UHV) chamber to get a **dilute atomic vapor** with around 10^6 atoms in 1 mm^3. This is achieved using traps to confine the atoms and cooling lasers with the following devices:

- **2 UHV chambers connected:** The first chamber performs the first confinement of the diluted vapor. Then, it is injected into a second chamber where it is confined and where the array of optical traps (*layout*) is loaded with atoms.
- **2D MOT (Magneto-Optical Trap):** Set of devices that act on the first UHV chamber to confine the atomic vapor along a single direction to be able to inject it into the second chamber. It is composed by:
  - The **Rb source** and the **oven**.
  - **3 lasers** at **780 nm**, 2 for laser cooling and 1 pusher beam. (See mechanism in the next item).

– **Magnetic coils** to confine the atoms in the direction along which the atoms are injected. (See mechanism in the next item).

A **CMOS camera** (Complementary Metal-Oxide-Semiconductor) is used to see the shape and size of the cloud measuring the absorbed light. (See figure 1).

- **3D MOT (Magneto-Optical Trap):** Set of devices that act on the second UHV chamber to slow down and confine the atom vapor in all directions before trapping them in an array of optical traps. They create a force over the atoms as $F_{3DMOT} = -\alpha v - \kappa z$, with v and z the velocity and position of the atom; and α, κ, constants. The 3D MOT is composed by:

  – **4 lasers** at **780 nm**: 2 vertical lasers are addressed in opposite directions. 2 horizontal ones are perpendicular to each other and they are reflected to get 2 pairs of lasers in opposite directions. **Four-quandrant photodiodes (4Qs)** are used to align the lasers accurately.

  Each laser is actually two overlapped beams, one slightly detuned from the other, and each one has a task: *cooling* and *repumping*. The reason why they are detuned is that they adress two different transitions between $5S_{1/2}$ and $5P_{3/2}$ hyperfine levels.

  The *cooling* mode uses **Doppler cooling** to slow the atoms down. Using a laser that is slightly detuned below an electronic transition, an atom travelling with velocity v towards a laser source is slowed down with a force $F = -\alpha v$ what gives an upper bound v in the cloud. The atom sees the laser with a higher frequency, unlike slow atoms, so it can promote and emmit a photon in a random direction, what in average slows down the ensemble.

  The *repumping* mode pumps the atom into the correct Zeeman sublevel $5S_{1/2}$ $(F = 2,\ M = 2)$, the ground state we need to perform Quantum Computing.

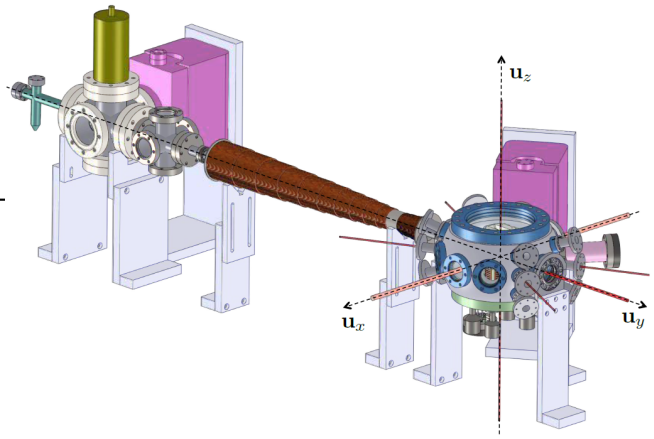

Figure 1: Scheme of the two UHV chambers and the 2D MOT and 3D MOT from [1].

  – **Quadrupole Coils:** It confines 10^6 atoms in 1 mm^3. Two pairs of anti-Helmholtz coils creates a magnetic field that varies linearly around the center and induces a Zeeman shifting that is linear with the position of the atom. The atoms that are far from the center can promote more easily because the level gap is smaller so they get slowed down more easily by Doppler cooling. This is translated into a brake force $F_{QC} = -\kappa z$ and, in average, they go to the center.

  It also counts with a **CMOS camera** to monitor the shape and size if the atom cloud. (See figure 1).

- **Spatial Light Modulator (SLM):** A **laser beam** at **815 nm** is driven to an **Acousto-Optic Modulator (AOM)** to control its intensity and, later, to the SLM, which uses holographic methods and diffraction techniques to create an optical trap array (layout), with a modifiable pattern. There is a 50% chance that a trap of the array is filled.

- **2 Acousto-optic laser beam deflector (AOD):** A **laser beam** at **852 nm** is driven to an AOM and, later, to the AOD. The 2 AOD steers the moving tweezer along 2 dimensions to move an atom between two traps and generate a 2D layout with a success rate over 99%. 4Qs

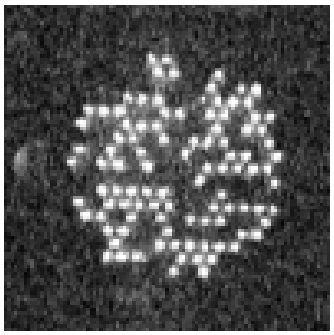

Figure 2: Atoms in the layout during the loading process, before rearrangement. EMCCD camera image.

are used for alignment.

Finally, in figure 2, we can see the signal obtained by the EMCCD camera while loading atoms, before the rearrangement.

2.2.2 Processing actuators:

To understand the devices used involved in quantum computation, we have to comprehend the quantum levels and the **mechanisms that Pasqal uses to describe and manipulate a two-level quantum system** (see figure 3).

The magnetic field that confines the atoms induce a Zeeman effect, a shift on the atom energy levels. This allows us to work with the hyperfine structure. This way, we have more levels to pick an appropiate 2-level system.

In our case, Pasqal uses a 3-level system in a regime that can be assimilated as a 2-level one. This is because we need a ground state and a Rydberg state to take the role of $|0\rangle$ and $|1\rangle$ but using an only transition we would need a UV laser that is very expensive and difficult to detune. Although in principle we do not need to detune the laser to perform computations, it is necessary to characterise some QPU features (as the optical trap depths) to prepare correctly all the parameters of the QPU.

The system consist of: $|g\rangle = |5S_{1/2}, F = 2, m_F = 2\rangle$, the *ground state*; $|i\rangle = |6P_{3/2}, F = 3, m_F = 3\rangle$, an *intermediate state*; and $|r\rangle = |60S_{1/2}\rangle$, the (excited) *Rydberg state*. There are two virtual states: $|v_i\rangle$, $|v_r\rangle$, that are states detuned from $|i\rangle$ and $|r\rangle$ respectively. $\Omega_1 \approx 420$ nm and $\Omega_2 \approx 1013$ nm

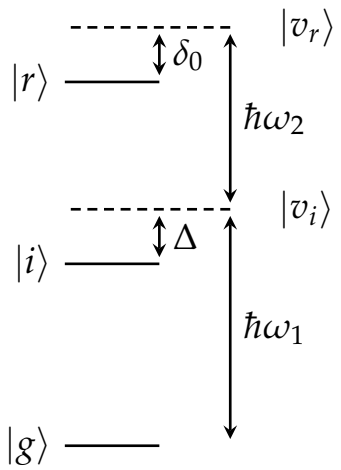

Figure 3: Level diagram of the qubits in Pasqal's QPUs. $|g\rangle = |5S_{1/2}, F = 2, m_F = 2\rangle$ is the ground state, $|i\rangle = |6P_{3/2}, F = 3, m_F = 3\rangle$ is an intermediate state, and $|r\rangle = |60S_{1/2}\rangle$ is the Rydberg (excited) state. There are two virtual states: $|v_i\rangle$, $|v_r\rangle$, that are states detuned from $|i\rangle$ and $|r\rangle$ respectively. $\hbar\omega_1$ and $\hbar\omega_2$ are such that $\lambda_1 \approx 420$ nm and $\lambda_2 \approx 1013$ nm for the frequencies of the lasers impinging on the atom. $\Delta \approx 450$ MHz is the first detuning frequency and δ_0, the total detuning frequency.

are the frequencies of the lasers impinging on the atom. $\Delta \approx 450$ MHz is the first detuning frequency and δ_0, the total detuning frequency. (See detailed theoretical model in section 3).

Pasqal's QPUs have two **Rydberg lasers** in charge of manipulating the quantum levels of the atoms:

- **840 nm:** Its frequency is doubled to 420 nm in a **Second-Harmonic Generator (SHG)** cavity in order to adress the $|g\rangle \rightarrow |i\rangle$ transition. A PasqCavity feedback change the frequency to the exact one that we want to apply, what is composed by a **Fabry-Perot cavity (F-P)** to measure exactly the laser frequency and a **Double-Pass AOM (DP AOM)** to change it. There is a detuning $\Delta \approx 450$ MHz so that the atom does not fall instantly into $|g\rangle$ and we can apply the second laser to have another transition without having an spontaneous emission from the intermediate level.
- **1013 nm:** It has a PasqCavity and a Fabry-Perot cavity similar to the prior case, without the SHG. In this step, there is a detuning

δ_{fixed}, fixed in the same way as before. Besides that, we can add a more accurate detuning δ_p using a Double-Pass AOM for different purposes, mainly to characterise the optical traps. Therefore, in total we have $\delta_{1013} = \delta_{fixed} + \delta_p$. After that, there is a **DP AOM**, an **ALS amplifier** and a **Single-Pass AOM** to modulate the power.

The total detuning is $\delta_0 = \Delta + \delta_{1013}$. However, the lasers induce an energy level-shift (*LS*) on the atom which, up to first order in $|\Omega/\Delta|$, is

$$\hbar\delta_i = \pm\Omega_i^2/(4\Delta_i) \tag{1}$$

with Δ_i the detuning in each transition. Ground and excited state detuning values are positive and negative, respectively.

Then, assuming a *LS* caused only by the Rydberg lasers (since the other confining lasers are usually switched off during the computation), the actual detuning is

$$\delta = \delta_0 + LS = \delta_0 + \frac{\Omega_{420}^2 - \alpha\Omega_{1013}^2}{4\Delta} \tag{2}$$

for which α is an experimental parameter that can be measured and it comes from an effect related to the high density of states around the Rydberg state. In this case, $\alpha = 1.86$. Our goal is having $\delta(\delta_p = 0) = 0$, with ($\delta_0 = 0$, $LS = 0$, $\delta = 0$) so that the total detuning is controlled by δ_p.

This quantum system of a single atom can be regarded as a 2-level system after some calculations with a frequency transition of

$$\Omega_{eff} = \frac{\Omega_1\Omega_2}{2\Delta} \tag{3}$$

Then the efficiency of 1-qubit gates can be achieved using Rabi and Ramsey oscillations. Pasqal is getting $\mathcal{F} > 0.995$.

2.2.3 Quantum register:

It is composed by the devices in the section *register actuators*, which are used to "read" the quantum state of the atoms. It is used an **Electron-Multiplying Charge-Coupled Device (EMCCD) camera**, that is highly sensitive to fluorescence photons. From the section *processing actuators* we know that the presence of an atom (bright signal) means reading the state $|0\rangle$ and abscence (dark signal), $|1\rangle$. Using the camera and false positive/negative functions we are able to read the state.

We highlight that the **FPD** (**Fast Photodiode**) and 4Qs are used to measure the power and alignment of the lasers. As with every laser, a wavemeter checks the final wavelength.

2.3 Support functions

To achieve a good control of the quantum system we need to monitor and control well every ambient factor that might affect it:

- **Vaccum in the UHV chamber:** It must be around 10 mbar.
- **EM field controllers:** It handles the unwanted electric and magnetic fields inside the chamber that might cause energy shifts on atoms. An *electronic rack* monitors the electric field with electrodes and the magnetic field with 3 coils, 1 for each direction of space.
- **Mechanical support:** It controls vibrations and mechanical deformations of the vaccum chamber.
- **Thermal Regulation:** It monitors the temperature of the *main frame system*, *electric system*, *laser system* and the *ambient conditions*. It maintains the temperature stable using an air-water cooling with a PID (proportional integral derivative) controller. It also controls the optical core benches and the 2 Rydberg benches using a Peltier thermoelectric cooler, compensating the heat generated by the AOMs and AODs.
- **Environment:** Humidity and pressure are uncontrolled phenomena that highly affect the performance of the QPU.
- **Sequencing:** It measures the synchronisation between trapping lasers and Rydberg lasers.
- **Power supply**
- **Data management**

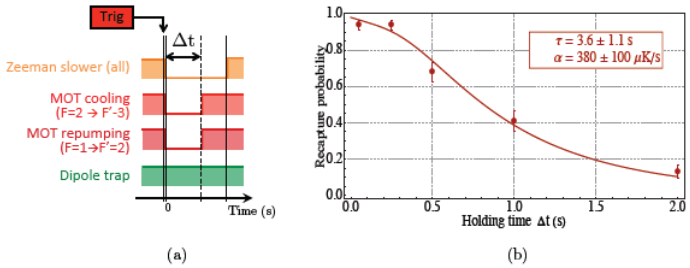

Figure 4: Lifetime trap measurements from [1].

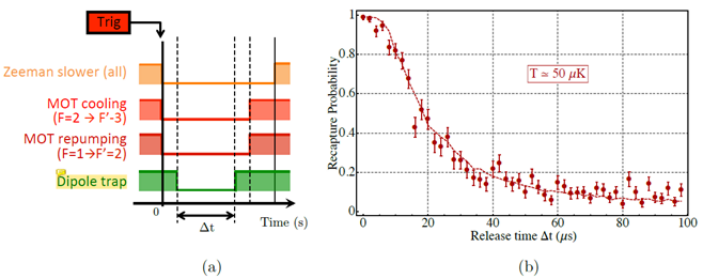

Figure 5: Single atom temperature measurements from [1].

2.4 Optical traps characterization

In order to fully understand the behaviour of the atoms, we need to monitor the optical traps. We can characterize 4 features:

2.4.1 Lifetime in the trap

The **lifetime in the trap** (τ) is the average time that the atoms remain in the dipole traps when the MOT lasers are switched off. As the operation time of a computation is around 100 ms, we need $\tau > 10$ s in order to have less than 1% of losses. In Pasqal, $\tau \approx 20$ s, twice the expected according to [1]. (See behaviour in the figure 4).

There are two loss mechanisms:

First, due to **collisions** with the molecules from the residual gas inside the vaccum chamber, with a surviving probability of:

$$P_{coll}(t) = e^{-t/\tau} \tag{4}$$

Second, due to the heating of the atoms, caused by the spontaneous scattering of impinging photons on the trapped atoms. According to B. Darquié [2]:

$$P_{heat}(t) = 1 - exp(-\frac{U_0}{k_B(T_0 + \alpha t)}) \cdot \tag{5}$$

$$\cdot (1 + \frac{U_0}{k_B(T_0 + \alpha t)} + \frac{U_0^2}{1k_B^2(T_0 + \alpha t)^2}) \tag{6}$$

with U_0, the trap depth; and α, the heat rate, increased temperature per second.

Then, the surviving probability is:

$$P(t) = P_{coll}(t) \cdot P_{heat}(t) \tag{7}$$

2.4.2 Single atom temperature

The **single atom temperature** is defined hereunder. When an atom is trapped, it will have a determined total energy E_i. The probability of an atom to have a certain energy is given by the thermal Boltzmann distribution according to the experiments [3]. Therby, the single atom temperature is defined as the temperature parameter of the distribution.

The protocol to measure it is:

1. Switch all the traps off except the dipole trap.
2. Switch the dipole trap off during Δt.
3. Switch the dipole trap on.
4. Switch the MOT traps on.
5. Measure the fluorescence to see the percentage of remaining atoms.

This is performed for a range of values of $\Delta t \in [0, 100]$ μs. Then Monte-Carlo simulations are performed and we choose the one with least minimum mean quadratic error. (See figure 5).

2.4.3 Trap oscillation frequencies

The **trap oscillation frequencies** are the frequencies of oscillation of the atoms in the trap. To measure them:

1. We switch all the traps off (confining trap and cooling lasers) so there is no level-shifting.
2. After a fixed time t_1 the dipole traps are switched on and off during a variable time $\Delta t = t_2 - t_1$.

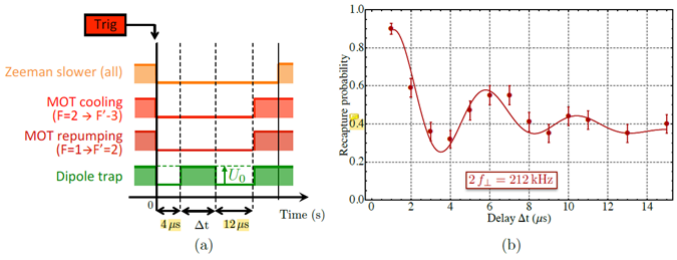

Figure 6: Atom oscillations measurements from [1].

3. All the traps are switched on again after a fixed time $t_3 - t_2$ and we measure the ratio of atoms that are still in the trap (*recapture rate*).

This gives an probability that oscillates with Δt and that has the frequency of the oscillations of the atoms. This is explained in detail in section 4. The figure 6 shows an example.

2.4.4 Trap depth

The **trap depth** depends on the power of the trapping laser. This dependence can be measured as follows. Once an atom is trapped, all the lasers are turned off except for the dipole trap and the repumping laser (the one that addresses the atom to the ground state $|g\rangle = |5S_{1/2}, F = 2, m_F = 2\rangle$ in order not to fall into a lower state). Then, the atom is brought to $|r\rangle = |60S_{1/2}\rangle$ performing a π-pulse, with a detuning δ_p, using the Rydberg lasers. Using a semiclassical approach and the rotating wave approximation, it can be proved that the dependence of the amount of atoms in the state $|r\rangle$ with δ_p has a lorentzian shape as:

$$N(t)dt = \frac{\Gamma}{2}\frac{I_p/I_{sat}}{1 + 4(\delta_p(t) - \delta_0(P_f))^2/\Gamma^2}dt \quad (8)$$

with Γ and I_{sat} parameters that depend on the atom species and transition.

The center of it (maximum $\delta_p = \tilde{\delta}_0$) is reached when the total detuning is zero: When $\delta_p = 0$ and we do not have traps, the system is tuned as $\delta = \delta_{0,Ry} + LS_{Ry} = 0$ with $\delta_{0,Ry} = \Delta + \delta_{1013} = \Delta + \delta_{fixed}$; $LS_{Ry} = 0$. If we have traps and detuning, then $\delta = \delta_{0,Ry} + \delta_p + LS_{Ry} + LS_{traps} = \delta_p + LS_{traps}$. Finally, if we measure the ratio of atoms in the Rydberg state in function of δ_p, the maximum is reached

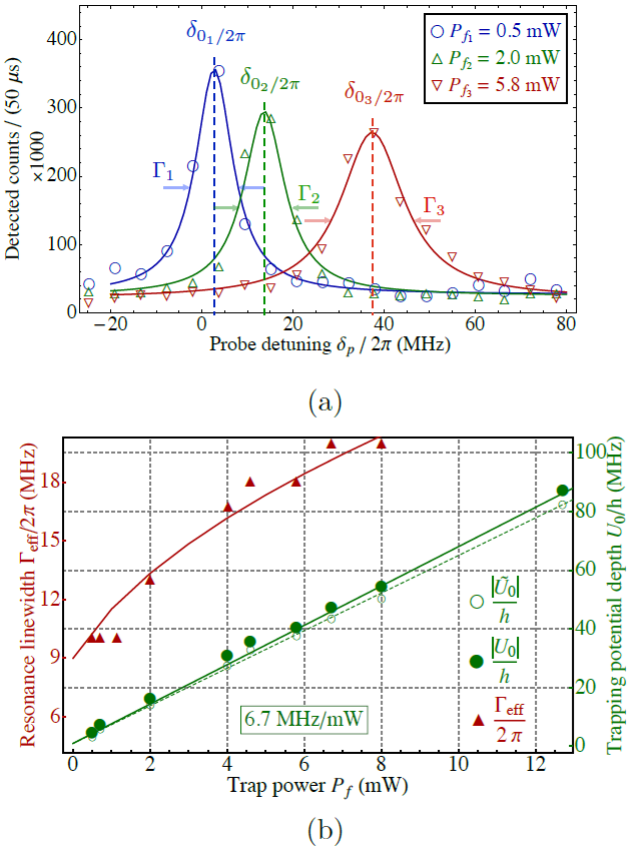

Figure 7: Trap depth measurements from [1].

when $\delta = 0$, then $\delta_p^{max} = -LS$, what gives the energy shifting due to the optical trap potential as $U_0/h = \delta_p^{max}/(2\pi)$. This is, the potential depth. See behaviour in figure 7.

3 Rabi Oscillations with two-photon transitions: theoretical model

In this section, I present the theory behind the Rabi oscillations using two-photon transitions in a 3-level system. I follow the article [4] and I develop the calculations that were omitted here.

Definition 3.1 (Two-photon transitions). *It is a second-order quantum mechanical process in which an atom (or other physical system) absorbs or emits two photons simultaneously, leading to a transition between two energy states. There can be a real or virtual intermediate state that allows this 2-step transition. This is a quantum model for light-matter interaction with 3 energy levels.*

There are 3 types of 2-photon transitions in a

3-level system: **Λ-type**, **V-type** and **Ξ-type**, also called *cascade*-type. This depends on the shape of the transition diagram: in order, they correspond to the intermediate state being the highest, lowest, or the middle energy state, respectively. The treatment is the same for all of them, but we only present the Ξ-type transition diagram, as it is the one used in Pasqal (figure 8).

Definition 3.2 (State energies)**.** *We will define the origin of energy as the energy of the ground state and, then, $\hbar\omega_i$ and $\hbar\omega_1$ are the* ***energies of the intermediate and excited states****.*

Definition 3.3 (Rabi frequencies)**.** *Given a 2-level system as a model of light-matter interaction with a sinusoidal coherent beam of light, it can be proved that the probability of finding the system in a state behaves as a sinusoidal function depending on the time that the laser was applied. Its frequency is the Rabi frequency* (Ω)*:*

$$\Omega = \frac{E_0 d_{01}^{\varepsilon}}{\hbar} \tag{9}$$

being E_0 the electric field amplitude of the coherent laser beam; and d_{01}^{ε}:

$$d_{01}^{\varepsilon} = \vec{\varepsilon}\langle 0|\vec{d}|1\rangle \tag{10}$$

with $|0\rangle$, $|1\rangle$ the states of the system, $\vec{d} = -e\vec{r}$ the dipole operator and $\vec{\varepsilon}$ the unit vector in the direction of the electric field amplitude vector.

Definition 3.4 ($\Omega_0, \Omega_1, \Delta_0, \Delta_1, \Delta$, ffi)**.** *$\Omega_0$ and Ω_1 are the Rabi frequencies of each transition $|0\rangle \to |i\rangle$, $|i\rangle \to |1\rangle$, respectively. Each transition is detuned an amount Δ_0 under and Δ_1 over the exact transition frequency but defined with the same sign. $\delta = \Delta_0 - \Delta_1$ is the total detuning and $\Delta = (\Delta_1 + \Delta_2)/2$ is the average detuning.*

Why can it be regarded as a 3-level system? We are considering a system with $\{|0\rangle, |i\rangle, |1\rangle\}$ energy levels and transitions between them. According to the Fermi Golden Rule, $\langle j|H_I|k\rangle$ is proportional to the transition probability of $|j\rangle \leftrightarrow |k\rangle$ at first order in perturbation theory. As we can assume that every other transition is very far detuned from the laser frequency, it is very unlikely that the atom promotes to any other state.

Finally, we will consider two **assumptions** to ease the calculations.

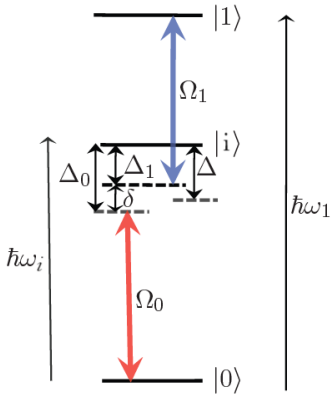

Figure 8: Ξ-type two-photon transition diagram [4]. $\hbar\omega_0$ and $\hbar\omega_1$ are the energies of the intermediate and excited states. Ω_0 and Ω_1 are the Rabi frequencies of each transition $|0\rangle \to |i\rangle$, $|i\rangle \to |1\rangle$. Each transition is detuned an amount Δ_0 under and Δ_1 over the exact transition frequency, respectively, but defined with the same sign. $\delta = \Delta_0 - \Delta_1$ is the total detuning and $\Delta = (\Delta_1 + \Delta_2)/2$ is the average detuning.

Definition 3.5 (Assumptions)**.**

- $|\Delta| \gg |\Delta_0|, |\Delta_1|$*: Pasqal sets the QPU like this so $|i\rangle$ is little populated and there is no spontaneous emission from this state to other ones. Therefore, as soon as the atom reaches $|i\rangle$, it will promote to $|1\rangle$ because the frequency with which photons reach the atom (due to the light intensity) is much higher than the spontaneous emission rate.*
- $|\delta/\Delta| \ll 1$*: The total detuning in the two-photon transition from $|0\rangle$ to $|1\rangle$ is nearly or exactly resonant so we only get the transition $|0\rangle \leftrightarrow |1\rangle$.*

3.0.1 Definition of the quantum system

Proposition 3.1. *We can describe the 3-level system with the Hamiltonian that is sum of the atom and atom-light interaction Hamiltonians. They are:*

$$H = H_{atom} + H_{AL} \tag{11}$$

$$H_A = \hbar \begin{pmatrix} 0 & 0 & 0 \\ 0 & \omega_1 & 0 \\ 0 & 0 & \omega_i \end{pmatrix} \tag{12}$$

$$H_{AL} = \frac{\hbar}{2}\begin{pmatrix} 0 & 0 & \Omega_0 e^{i\omega_{L0}t} \\ 0 & 0 & \Omega_1 e^{i\omega_{L1}t} \\ \Omega_0^* e^{-i\omega_{L0}t} & \Omega_1^* e^{-i\omega_{L1}t} & 0 \end{pmatrix} \quad (13)$$

Proof. From Maxwell equations, it can be proved that the Hamiltonian of a system consisting of a light beam impinging on an atom is the sum of the atom Hamiltonian plus an interaction Hamiltonian as $H = H_A + H_{AL}$ with $H_{AL} = -\hat{\vec{d}}\vec{E}$, $\hat{\vec{d}} = -e\hat{\vec{r}}$ the dipole operator and

$$\vec{E}(t) = \vec{E}_{00}\cos(\omega_{L0}t + \varphi_0) + \vec{E}_{01}\cos(\omega_{L1}t + \varphi_1) \quad (14)$$

the electric field of the beam. The **dipole approximation** is applied here. Let's write the amplitude vector as an amplitude times a unit vector $\vec{E}_{0j} = E_{0j}\,\vec{\varepsilon}_j$. It can be proved that we reach the same result if $\varphi_i = 0$.

We will define:

Definition 3.6 ($\vec{d}_{kj}$, d^{ε}_{kj})**.**

$$\vec{d}_{kj} := \langle k|\hat{\vec{d}}_{kj}|j\rangle \quad (15)$$

$$d^{\varepsilon}_{kj} := \langle k|\vec{\varepsilon}\,\hat{\vec{d}}_{kj}|j\rangle \quad (16)$$

Remark:

i) $d_{jk} = d^*_{kj} = d_{kj} = d^*_{jk} \in \mathbb{R}$

ii) As the atom wavefunction for a given state (ψ_n) has a defined parity, then $\psi^*_n\psi_n$ has even parity; and as $\vec{r}$ is an odd function:

$$\vec{d}_{jj} = \langle j|\hat{\vec{d}}|j\rangle = \int \psi_n(\vec{r})^*(-e\hat{\vec{r}})\psi_n(\vec{r}) = \vec{0} \quad (17)$$

Now, we will use the **rotating-wave approximation** to get a simpler Hamiltonian that approximately describes the same system.

We will change to the interaction picture

$$H^I = e^{\frac{iH_A t}{\hbar}} H\, e^{\frac{-iH_A t}{\hbar}} = H^I_A + H^I_I \quad (18)$$

But $H^I_{atom} = H_{atom}$ because it conmutes with itself. Moreover, using that

$$e^{\frac{iH_A t}{\hbar}} = \begin{pmatrix} 1 & 0 & 1 \\ 0 & e^{i\omega_1 t} & 0 \\ 0 & 0 & e^{i\omega_i t} \end{pmatrix} \quad (19)$$

and

$$H_{AL} = -\vec{E}\sum_{j,k}\langle j|\hat{\vec{d}}|k\rangle|j\rangle\langle k| = -\vec{E}\begin{pmatrix} 0 & \vec{d}_{01} & \vec{d}_{0i} \\ \vec{d}_{10} & 0 & \vec{d}_{1i} \\ \vec{d}_{i0} & \vec{d}_{i1} & 0 \end{pmatrix} \quad (20)$$

we have that

$$H^I_{AL} = -\vec{E}\begin{pmatrix} 0 & \vec{d}_{01}e^{i\omega_{01}t} & \vec{d}_{0i}e^{i\omega_{0i}t} \\ \vec{d}_{10}e^{i\omega_{10}t} & 0 & \vec{d}_{1i}e^{i\omega_{1i}t} \\ \vec{d}_{i0}e^{i\omega_{i0}t} & \vec{d}_{i1}e^{i\omega_{i1}t} & 0 \end{pmatrix} \quad (21)$$

with $\omega_{jk} := \omega_j - \omega_k$.

So, developing $\vec{E}$, the matrix elements of H^I_{AL} are

$$(H^I_{AL})_{jk} = \hbar\sum_{j,k}\Big[\Omega_0^{j,k}\cos(\omega_{L0}t) + \Omega_1^{j,k}\cos(\omega_{L1}t)\Big]e^{i\omega_{jk}t}|j\rangle\langle k| \quad (22)$$

with:

Definition 3.7 ($\Omega^{j,k}_{\alpha}$)**.** *We define* $\forall\alpha \in \{0,1\}$, $\forall j,k \in \{0,1,i\}$,

$$\Omega^{j,k}_{\alpha} := \frac{E_{0\alpha}d^{\varepsilon_\alpha}_{jk}}{\hbar} \quad (23)$$

$$\Omega_0 := \frac{E_{00}d^{\varepsilon_0}_{0i}}{\hbar} \quad (24)$$

$$\Omega_1 := \frac{E_{01}d^{\varepsilon_1}_{i1}}{\hbar} \quad (25)$$

Expressing the cosines as sum of complex exponentials:

$$(H^I_{AL})_{jk} = \hbar\sum_{j,k}\Big[\Omega_0^{j,k}\frac{1}{2}\left(e^{i(\omega_{jk}-\omega_{L0})t} + e^{i(\omega_{jk}+\omega_{L0})t}\right) + \Omega_1^{j,k}\frac{1}{2}\left(e^{i(\omega_{jk}-\omega_{L1})t} + e^{i(\omega_{jk}+\omega_{L1})t}\right)\Big]|j\rangle\langle k| \quad (26)$$

Now, we introduce the **rotating-wave approximation**:

Definition 3.8 (Rotating-wave approximation)**.** *We will perform an approximation in the equation 26. Given* $j,k \in \{0,1,i\}$, ω_{jk} *represents a transition energy. We assume that* $\omega_{L0} \neq \omega_{L1}$ *are very different. We also assume that* ω_{L0} *is near resonance with* ω_{i0} *and that* ω_{L1} *is near resonance with* ω_{1i}*. Therefore, both* ω_{L0} *and* ω_{L1} *are far detuned from* ω_{01}*. This means that* $\forall j,k \in \{0,1,i\}$, $\alpha \in \{0,1\}$*:*

$$|\omega_{i0} - \omega_{L0}|, |\omega_{1i} - \omega_{L1}| \ll |\omega_{jk} \pm \omega_{L\alpha}| \quad (27)$$

for any other combination of indices j, k, α (save change of sign).

Hence, $\forall j,k \in \{0,1,i\}$, the terms at right in 27 are considered rapidly oscillating and on any appreciable time scale, the oscillations will quickly average to 0. This is due to the fact that, when we solve the Schrödinger equation in the interaction picture, the integral of the quickly oscillating terms are negligible in comparison with the slowly oscillating ones. That leaves:

$$H^I_{AL} = \frac{\hbar}{2}\begin{pmatrix} 0 & 0 & \Omega_0 e^{i\Delta\omega_0 t} \\ 0 & 0 & \Omega_1 e^{i\Delta\omega_1 t} \\ \Omega_0^* e^{-i\Delta\omega_0 t} & \Omega_1^* e^{-i\Delta\omega_1 t} & 0 \end{pmatrix} \tag{28}$$

with $\Delta\omega_0 := \omega_{L0} - \omega_{i0}$ and $\Delta\omega_1 := \omega_{L1} - \omega_{1i}$

Finally, returning to the Schrödinger picture, we have the matrix that we wanted.

□

3.0.2 System in the interaction picture

As H_{AL} is time-dependent in the Schrödinger picture, we will redefine a separation if the Hamiltonian and change to the interaction picture. This will give a non time-dependent Hamiltonian.

Remark: In the interaction and Schrödinger picures, the absolute value of the wavefunction coefficients are the same.

Definition 3.9 (H_0, H_I)**.** *We can express the Hamiltonian as:*

$$H = H_0 + H_I \tag{29}$$

$$H_0 = \hbar\begin{pmatrix} \delta/2 & 0 & 0 \\ 0 & \omega_1 - \delta/2 & 0 \\ 0 & 0 & \omega_i - \Delta \end{pmatrix} \tag{30}$$

$$H_I = \hbar\begin{pmatrix} -\delta/2 & 0 & \frac{\Omega_0}{2} e^{i\omega_{L0}t} \\ 0 & \delta/2 & \frac{\Omega_1}{2} e^{i\omega_{L1}} \\ \frac{\Omega_0^*}{2} e^{-i\omega_{L0}t} & \frac{\Omega_1^*}{2} e^{-i\omega_{L0}t} & \Delta \end{pmatrix} \tag{31}$$

Proposition 3.2. *The Hamiltonian in the interaction picture is:*

$$H^I = e^{\frac{iH_0 t}{\hbar}} H\, e^{\frac{-iH_0 t}{\hbar}} = H_0^I + H_I^I \tag{32}$$

$$H_0^I = e^{\frac{iH_0 t}{\hbar}} H_0\, e^{\frac{-iH_0 t}{\hbar}} = H_0 \tag{33}$$

$$H_I^I = e^{\frac{iH_0 t}{\hbar}} H_I\, e^{\frac{-iH_0 t}{\hbar}} = \frac{\hbar}{2}\begin{pmatrix} -\delta & 0 & \Omega_0 \\ 0 & \delta & \Omega_1 \\ \Omega_0^* & \Omega_1^* & 2\Delta \end{pmatrix} \tag{34}$$

Proof.

- $H_0^I = H_0$ because $[H_0, H_0]$, so $[H_0, e^{\frac{iH_0 t}{\hbar}}]$ and the exponential terms cancel out.
- Regarding H_I^I, we calculate $e^{\frac{iH_0 t}{\hbar}}$ and apply the definition. As H_0 is a diagonal matrix:

$$e^{\frac{iH_0 t}{\hbar}} = \begin{pmatrix} e^{\frac{i\delta t}{2}} & 0 & 0 \\ 0 & e^{i(\omega_1 - \frac{\delta}{2})t} & 0 \\ 0 & 0 & e^{i(\omega_i - \Delta)t} \end{pmatrix} \tag{35}$$

  Applying matrix multiplications and using the definition 3.9 of H_I and the detuning magnitudes relations from the definition 3.4 we get the result we wanted.

□

The system evolves according to the Schrödinger equation in the interaction picture as

$$i\hbar\frac{\partial}{\partial t}\psi_I(t) = H_I^I \psi_I(t) \tag{36}$$

Therefore, $\forall j \in \{0, i, 1\}$

$$|c_j^I(t)|^2 = |\langle j|\psi_I(t)\rangle| = |\langle j|e^{iH_0 t}|\psi(t)\rangle| = |c_j(t)|^2 \tag{37}$$

so it suffices to obtain $c_j^I(t)$ to get $|c_j(t)|$. We will omit the superscript I to ease the notation.

3.0.3 Adiabatic elimination method

To ease the calculations we will apply a second approximation:

Definition 3.10 (Adiabatic elimination)**.**

- *The wavefunction will evolve to a state with $c_i \approx 0$ because it is far detuned by Δ (see assumptions in 3.5).*

- *Therefore, we can assume that* $c_i(t=0) \approx 0$ *and it will remain almost zero:* $c_i(t) \approx 0,\ \forall t \geq 0$. *Then, we can state:*

$$\partial_t c_i(t) = 0 \tag{38}$$

Remark: c_i *is the coefficient of the intermediate state.*

Using the *adiabatic elimination* 3.10, the Schrödinger equation 36, and projecting over $|i\rangle$ we have:

$$2i\,\partial_t c_i(t) = \langle i|H_I^I|\psi_I\rangle = \Omega_0^* c_0(t) + \Omega_1^* c_1(t) + 2\Delta c_0(t) = 0 \tag{39}$$

Finally, we can express the intermediate state as a linear combination of the other states:

$$c_e(t) = -\frac{\Omega_0^* c_0(t) + \Omega_1^* c_1(t)}{2\Delta} \tag{40}$$

Proposition 3.3. *The adiabatic elimination gives an effective* 2×2 *Hamiltonian for the evolution of* $|0\rangle$ *and* $|1\rangle$ *as:*

$$H_{eff} = -\frac{\hbar}{2}\begin{pmatrix} \delta + \frac{|\Omega_0|^2}{2\Delta} & \frac{\Omega_0\Omega_1^*}{2\Delta} \\ \frac{\Omega_0^*\Omega_1}{2\Delta} & -\delta + \frac{|\Omega_1|^2}{2\Delta} \end{pmatrix} \tag{41}$$

Proof. The evolution of a system is given by the Schrödinger equation, that depends only on the (interaction) Hamiltonian (in the interaction picture). Using the equation 40 and applying H_I^I over a generic state:

$$H_I^I\psi_I = \frac{\hbar}{2}\begin{pmatrix} -\delta & 0 & \Omega_0 \\ 0 & \delta & \Omega_1 \\ \Omega_0^* & \Omega_1^* & 2\Delta \end{pmatrix}\begin{pmatrix} c_0^I \\ c_1^I \\ c_i^I \end{pmatrix}$$

$$= \begin{pmatrix} -\delta c_0^I - \frac{|\Omega_0|^2 c_0^I}{2\Delta} - \frac{\Omega_0\Omega_1^* c_1^I}{2\Delta} \\ \delta c_1^I - \frac{\Omega_0^*\Omega_1 c_0^I}{2\Delta} - \frac{|\Omega_1|^2 c_1^I}{2\Delta} \\ 0 \end{pmatrix}$$

This last vector can be expressed as a multiplication of a 2×2 matrix by a 2×1 vector as $H_{eff}\begin{pmatrix} c_0^I & c_1^I \end{pmatrix}^T$ by neglecting the $|i\rangle$ row. □

3.0.4 Evolution of the quantum system

After these assumptions and approximations, we have a non time-dependent 2×2 quantum system for which we can calculate the eigenvalues and vectors. Finally, we use the Schrödinger equation 36 to get the evolution. We omit the long calculations for simplicity.

Definition 3.11 (Eigenenergies of the atom)**.** *The system eigenenergies are:*

$$E_\pm = -\frac{\hbar}{8\Delta}\left(|\Omega_0|^2 + |\Omega_1|^2\right) \pm \frac{\hbar}{2}\Omega_R \tag{42}$$

with

$$\Omega_R^2 = \left(\frac{|\Omega_0|^2 + |\Omega_1|^2}{4\Delta}\right)^2 + \frac{\delta}{2\Delta}\left(|\Omega_0|^2 - |\Omega_1|^2\right) + \delta^2 \tag{43}$$

Definition 3.12 (Eigenvectors of the atom)**.**

$$|-\rangle = \begin{pmatrix} -\frac{\Omega_0\Omega_1^*}{2\Delta} \\ \delta + \frac{|\Omega_0|^2 - |\Omega_1|^2}{4\Delta} - \Omega_R \end{pmatrix} \tag{44}$$

$$|+\rangle = \begin{pmatrix} -\frac{\Omega_0\Omega_1^*}{2\Delta} \\ \delta + \frac{|\Omega_0|^2 - |\Omega_1|^2}{4\Delta} + \Omega_R \end{pmatrix} \tag{45}$$

Finally, we can solve the Schrödinger equation 36 by diagonalizing the system of 2 differential equations, but we already have the eigenvalues and eigenvectors, so changing the basis we have:

$$i\hbar\begin{pmatrix} \dot{c}_- \\ \dot{c}_+ \end{pmatrix} = \begin{pmatrix} E_- & 0 \\ 0 & E_+ \end{pmatrix}\begin{pmatrix} c_- \\ c_+ \end{pmatrix} \tag{46}$$

The **general solution** is

$$|\psi(t)\rangle = K_- e^{\frac{-iE_-t}{\hbar}}|-\rangle + K_+ e^{\frac{-iE_+t}{\hbar}}|+\rangle \tag{47}$$

Assuming the initial conditions $c_0(t=0) = 1$, $c_1(t=0) = 0$ and taking into account that $c_0^I(t) = \langle 0|\psi(t)\rangle$, $c_1^I(t) = \langle 1|\psi(t)\rangle$:

$$c_0(t) = e^{i\theta t}\left\{\cos\left(\frac{\Omega_R}{2}t\right) - i\left[\frac{\delta}{\Omega_R} + \frac{|\Omega_0|^2 - |\Omega_1|^2}{4\Delta\Omega_R}\right]\sin(\frac{\Omega_R}{2}t)\right\} \tag{48}$$

$$c_1(t) = -e^{i\theta t}\left[\frac{|\Omega_0|^2|\Omega_1|^2}{\Omega_R\Omega_0\Omega_1^*}\frac{1}{2\Delta}\right]\sin\left(\frac{\Omega_R}{2}t\right) \tag{49}$$

with

$$\theta = \frac{|\Omega_0|^2 + |\Omega_1|^2}{8\Delta} \tag{50}$$

Therefore,

$$|c_1(t)|^2 = \frac{|\Omega_0|^2|\Omega_1|^2}{4\Delta\Omega_R^2}\,\frac{1}{2}\left(1 - \cos(\Omega_R t)\right) \tag{51}$$

3.0.5 Rabi oscillations with amplitude 1

The Rabi oscillations amplitude is $0 \leq \frac{|\Omega_0|^2|\Omega_1|^2}{4\Delta\Omega_R^2} \leq 1$.

Proposition 3.4. *If* $\delta = 0$,

i $\frac{|\Omega_0|^2|\Omega_1|^2}{4\Delta\Omega_R^2} = \frac{4|\Omega_0|^2|\Omega_1|^1}{(|\Omega_0|^2+|\Omega_1|^2)}$

ii $\frac{|\Omega_0|^2|\Omega_1|^2}{4\Delta\Omega_R^2} = 1 \Leftrightarrow |\Omega_0| = |\Omega_1|$

Proof.

i Substituting in Ω_R according to the equation 43.

ii Using Cauchy-Schwartz inequality.

□

Proposition 3.5. *If* $\delta = \frac{|\Omega_1|^2-|\Omega_0|^2}{4\Delta}$

i $\frac{|\Omega_0|^2|\Omega_1|^2}{4\Delta\Omega_R^2} = 1$

ii $\Omega_R = \frac{|\Omega_0||\Omega_1|}{2\Delta}$

Proof. Substituting in Ω_R according to the equation 43. □

Conclusion: Modulating δ so that it fulfils the relation in the proposition 3.5, we can have Rabi oscillations with amplitude 1 without being forced to set $\Omega_0 = \Omega_1$.

4 Simulation of the trap oscillation frequencies

4.1 My role

During a meeting, the team presented several results to characterise the traps. These appear in the article [1], one of the main articles that the team follows to describe the QPU performance. At the section 2.3, it describes 4 parameters of the atom traps and how to measure them. Concretely, these are the ones explained in section 2.4.

Most of them could be explained successfully, with satisfactory results, as for the lifetime with around $2-3$ times better than what the article presents: $\tau \approx 20$ s. However, the damping behaviour in figure 6 was still in process of being studied and understood. I decided to work on this in parallel and compare my results with my colleague to check pros and cons for each model.

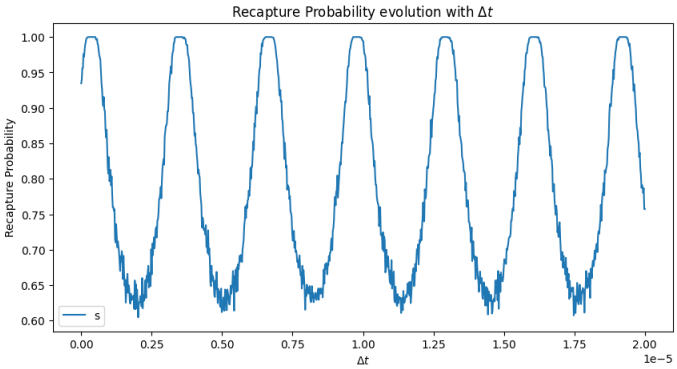

Figure 9: Monte-Carlo simulation of the recapture probability for obtaining the atom oscillation frequency using a harmonic oscillator in the intermediate step and a dipole potential at the end.

4.2 Theoretical model and simulation

As explained in section 2.4.3, to measure the oscillation frequency of the atom in the trap, it can be performed the protocol in figure 6.

The model that I present to describe this process, consists of four steps:

1. Oscillation with a determined energy during a time t_0 due to the presence of a potential well.
2. Free space propagation until t_1.
3. Oscillation with a determined (different) energy until t_2 due to the presence of a potential well.
4. Free space propagation until t_3.

After the dipole trap is switched off, the atom moves with constant velocity; and if $t_1 - t_0$ is large enough, it will go out the trap. This happens when the sum of kinetic energy is greater than the potential energy in absolute values, setting the origin of energy for a free atom with null velocity.

At the beginning, I used the harmonic oscillator potential for $t \in [0, t_0]$ and $t \in [t_1, t_2]$ but it

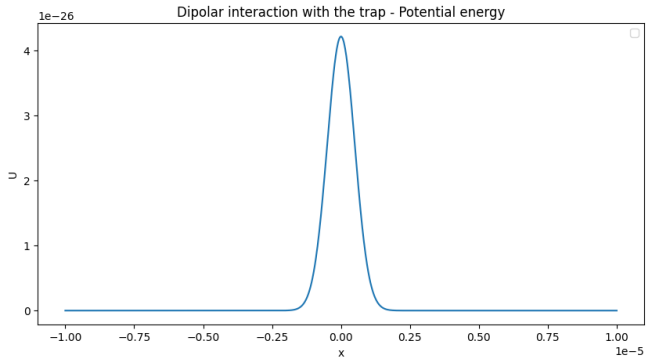

Figure 10: Dipole potential energy for $U_0 > 0$.

did not show any damping property (see figure 9) because it is an infinite well and, obviously, it cannot represent the real trap potential, save when the atom has low enough energy as in the first step. It was used the dipole potential instead (see figure 10):

$$U(x) = U_0\, e^{-2x^2/w^2} \tag{52}$$

According to the article [3], the energy distribution of an atom in a trap follows the Boltzmann distribution for a given temperature (what is used to define and calculate the single atom temperature). The simulation was done for a 1D system so the distribution is:

$$f(E) = \frac{1}{\sqrt{2\pi E k_b T}} e^{-E/(k_b T)} \tag{53}$$

Finally, a Monte-Carlo simulation was carried out to obtain the oscillation frequency. Given an energy, the position and velocity of the atom in the instant t_0 cannot be known so it is a probabilistic process. The initial sample at t_0 is obtained setting the atom at the bottom of the well with a velocity given by $E = 1/2mv^2$ and picking uniformly distributed random numbers in $[0, T(E)]$, with T the period of oscillation, which depends on the energy.

After that, the evolution of the sample is simulated until t_2 and then it is checked the recapture condition. To achieve this we used the *Verlet Algorithm* because it is widely-know for conserving the energy well and being simple, and we want this because our escaping condition depends on the energy. We can see the results in the figure 11.

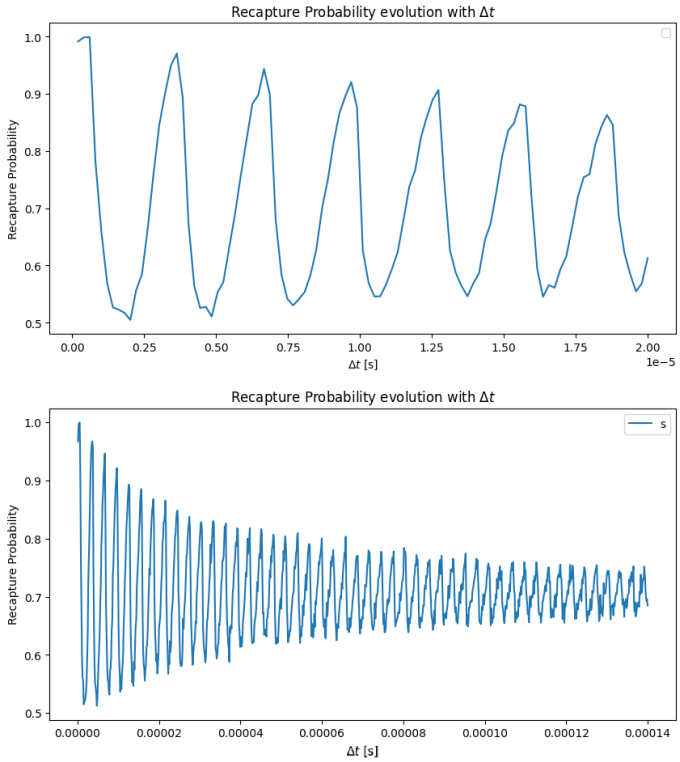

Figure 11: Monte-Carlo simulation of the recapture probability for obtaining the atoms oscillation frequency using a dipole potential.

4.3 Conclusion

The case in which we used the harmonic potential did not show any damping because we have no loss of particles until the moment of measurement. Then the maximums have a value of 1 because no particle can escape (see figure 9).

In the dipolar potential case we have 2 main behaviours that we will explain.

1. **Oscillations:** First, the points (atoms) in the phase diagram (position-velocity) are rotating. After the dipolar trap is switched off, the atoms conserve their velocity, what translates into a spread along the position axis in the phase diagram (position-velocity), describing an ellipse. When it is turned on again, the points start to rotate again (see figure 12). The recapture probability is maximum when the long axis of the ellipse is horizontal, and minimum when it is vertical. Then, these oscillations give the atom oscillation frequency in a trap. This is because the fast atoms will move to a far position if

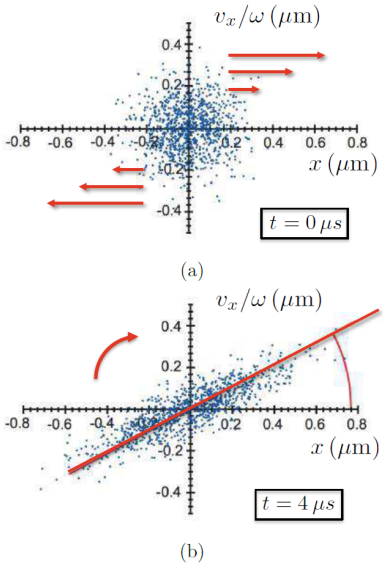

Figure 12: Phase diagram in the measurement of atom oscillation frequencies [1].

$t_3 - t_2$ is long enough. Hence, in the intant t_3, they will have a big kinetic energy since it was conserved, and a big potential energy, since it the atom is far from the trap center.

Equivalent explanation: The probability of finding a particle in the dipolar trap is very high for maximum positions at any moment, because their velocities here are minimum. Then, during the off periods of the trap, these bunches of possible particle positions move slowly towards the center or out the trap (depending the direction of their velocities). When the trap is switched on, the particles start oscillating again but with more spread energies. After switching off a second time, if the time $t_2 - t_1$ is such that this bunch of atoms is at the center in t_2, they will escape from the well with high energy if $t_3 - t_2$ is long enough to let them escape. This is because in the second time we switch the trap on, the particles in the bunch will have a big kinetic energy and they will be very far from the trap center so, they will also have a big potential energy, and they escape. This minimum recapture probability is repeated over time with the atom oscillation frequency as $\Delta t = t_2 - t_1$ changes.

2. **Damping:** During off times, the bunch at maximum positions suffers a spreading so there will be more atoms far from the edges from the trap, then more at the center of it, what means more with high kinetic energy. The particles that are near the center of the trap will have high velocities and will escape when the trap is switched off during enough times ($t_1 - t_0$ and $t_3 - t_2$). Therefore, there is a damping and, neglecting the oscillations behaviour, the number of lost particles will only depend on the spreading, namely, on $t_1 - t_0$ and $t_3 - t_2$. Thereby, these parameters determine the value to which the recapture rate tends (see figure 11).

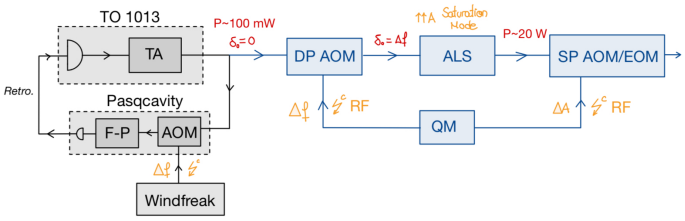

Figure 13: Laser setup scheme.

Given the theoretical model, we can predict that the **oscillations** in the plot does not depend on t_1, t_2, t_3, but on the mean energy value (**temperature**). Therefore, it depends on the mean period value of the atoms in the traps. We can also predict that the value to which the recapture rate **converges changes with different choices of** t_0, t_1 t_2, t_3.

We can conclude that the model satisfies the experimental behaviour.

5 Acquisition device calibration. Anomalies characterization.

In this section it is presented the main task that, as an intern, I performed in Pasqal. It consisted of characterising the Rydberg laser square pulses in charge of changing the quantum states of the atoms (qubits).

5.1 Laser system operation

In the figure 13 it is showed the main components that manipulate a laser.

The **black part** was already detailed in 2.2.2 and it is in charge of obtaining a constant power

and detuning $P \approx 100$ mW, $\delta_0 = 0$. It is considered to work correctly. The **blue part** detunes the laser with a DP AOM. Later, the ALS amplifier maintains the power stable at $P \approx 20$ W before the amplitude modulation. Finally, the amplitude is modulated with a Single-Pass AOM (SP AOM) for the case of the 1013 nm beam or with an EOM (lesser rise/fall time for short pulses and better resolution), for the 420 nm beam.

Windfreak and *Quantum Machine* are two devices that provide a radiofrequency (RF) electric pulse to control the AOMs (detuning and amplitude modulation).

5.2 Pulse sequence modes

Pulse sequences can be defined in two different modes: as a *one-photon transition* or a *two-photon transition*.

- **One-photon transition:** Rydberg lasers are added independently to the sequence and we have to specify the characteristics of both (duration, power, etc.). Each one addresses a different transition $|0\rangle \rightarrow |i\rangle$, $|i\rangle \rightarrow |1\rangle$. In this case, the input power is given in units of Rabi frequency and the *Quantum Machine* device performs the conversion to the electrical power that will make the laser work producing the input Rabi frequency.

  Instead of assuming the relation bewteen intensity, power and beam area $I = P \cdot A$, which is too simple, it is used an experimental relation:

  $$\Omega = \Gamma \sqrt{\frac{1}{2} \frac{I}{I_{sat}}} \tag{54}$$

  with Γ and I_{sat}, parameters that depend on the atom species and the transition.

- **Two-photon transition:** It combines both lasers as if we had an only laser that addressed the transition $|0\rangle \rightarrow |1\rangle$. We need to specify duration of the pulse and power as a whole. The input power is given in units of effective Rabi frequency as in 3.

5.3 Measurements for laser characterization

To characterise the pulses, firstly, I changed the program in charge of reading Rydberg laser pulses data so it can be used with the new device called *Spectrum*.

Later, my supervisor showed me how to create new programs in PasqOS, the Operative System to control the QPU, and I designed 3 different square pulses sequences to caracterise them. These programs were:

- **Red Pulse Detuning Scan:** There is a Double-Pass AOM to detune the 1013 nm pulse to be able to characterise QPU's features. This program records the power of the 1013 nm Rydberg laser in function of time for different detuning values. The laser power is recorded by the *Spectrum* device as voltage. The aim of this is to check possible anomalies in the behaviour of the square pulses for different detuning values.

- **Pulse Duration Scan:** We need to see how the consistency of a square pulse changes with the duration of the pulse. Thereby, we scan laser powers for different duration pulses for both Rydberg lasers. I did not have time to take the measurements so I could not do any analysis.

- **Pulse Amplitude Scan:** It scans the amplitude of the power laser in voltage units for different input Rabi frequencies. The goal of it is explained hereunder:

Theoretically, the effective Rabi frequency has a dependence as in 3 or, experimentally, as in 54.

But the laser diode can emit a slightly different power from the desired one and we need to calibrate that as:

$$(V_{meas,0}, V_{meas,1}) = f(\Omega_{input}) \tag{55}$$

In the end, we want to measure the experimental Rabi frequency Ω_{Rabi}, while using the *Pulse Amplitude Scan* program to be able to calibrate the effective laser power:

$$\Omega_{meas} = g(V_{meas,0}, V_{meas,1}) \tag{56}$$

With the expressions 55 and 56, we will be able to get the relation:

$$\Omega_{meas} = h(\Omega_{input}) \tag{57}$$

and implementing this in the laser power controller we can apply a Rabi frequency without measuring it.

Note: In the end I did not have time to fit g because there was not a program to scan many Rabi frequencies at once so I could not take the measurements.

5.4 Data analysis

Firstly, I programmed functions in python to measure the square pulse parameters: on and off time, rise and fall time, pulse duration and value of the constant voltage. With them, I would be able to **discern if the (noisy) signals were good square pulses**, and carry out both analysis presented before. The parameters were defined as:

Definition 5.1 (On time. Off time:)**.** *They are the instants at which we start to record light and we stop recording light during a pulse sequence. There can be several of them for each laser sequence depending on how it was defined.*

Definition 5.2 (On plateau time. Off plateau time:)**.** *The on plateau time is the first moment after an on time with zero signal derivative. Similarly, the off plateau time is the first moment just before an off time instant with zero signal derivative.*

Definition 5.3 (Filtered signal:)**.** *To mitigate the noise, the measurement was filtered. Thus, the true value of the signal in an instant of time was considered the mean value of a batch of measurements around it. The batch size (B) could be controlled to get a good signal, not too smooth, not too noisy. The filtered signal is then:*

$$x^{filt}_{i+B\,\mathbf{div}\,2} = \frac{1}{B}\sum(x_i, ..., x_{i+B}) \tag{58}$$

with **div**, *the integer division.*

It was considered that there was light signal when the voltage was greater than 3 times the resolution of the aparatus (Spectrum).

Definition 5.4 (Filtered signal derivative:)**.** *The filtered signal derivative was treated as:*

$$x'^{filt}_{i+B\,\mathbf{div}\,2} = \frac{1}{B}(x_{i+B} - x_i) \tag{59}$$

with **div**, *the integer division.*

The derivative was considered 0 if the absolute value of the finite difference presented was lesser than 0.0001.

5.4.1 Pulse detuning analysis

In the figure 14 we see 3 of the pulses, in order: $\delta = -62.83$ rad$/\mu s$, $\delta = 0.63$ rad$/\mu s$ and $\delta = -62.83$ rad$/\mu s$. These are the measurements with largest negative detuning, approximately zero detuning and largest positive detuning, respectively.

As we can see in 14, there is a **tilting** at the plateau in every pulse, that was equal for every measurement, while the desired behaviour is to be constant. Moreover, **oscillations at the plateau** were observed depending on $\delta > 0$ as:

i) $\delta \geq 13.32$ rad$/\mu s$: The oscillation frequency increased with δ while the amplitude was constant.

ii) $\delta \approx 0$ rad$/\mu s$: The plateau was constant.

iii) $\delta \leq -12.06$ rad$/\mu s$: It looked constant at first but there are oscillations with symmetrical frequencies as for $\delta \geq 13.32$. The oscillations are around 3 times smaller.

We can observe better the oscillations in the figure 15, where the data was filtered.

Tilting: The tilting was **removed** by subtracting the **linear regression of each plateau**. It was **equal for all** the plateaus because the variations in the slope and y-intercept coefficients could be explained by the data statistical dispersion (standard deviation).

Plateau mean voltage: From these data we can obtain the plateau **mean** voltage and its **standard deviation** as shown in 16. The voltage decreases with $\delta \neq 0$ and it has a quadratic behaviour (see table 1). It is not centered at $\delta = 0$ rad$/\mu s$, but around $\delta \approx -3.39$ rad$/\mu s$. This was unexpected as the devices should work symmetrically for positive and negative detuning values. The fitting coefficients are in 1.

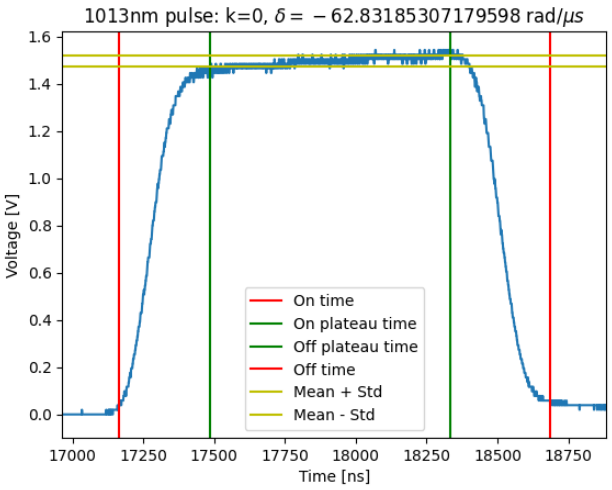

(a) $\delta = -62.83$ rad$/\mu s$

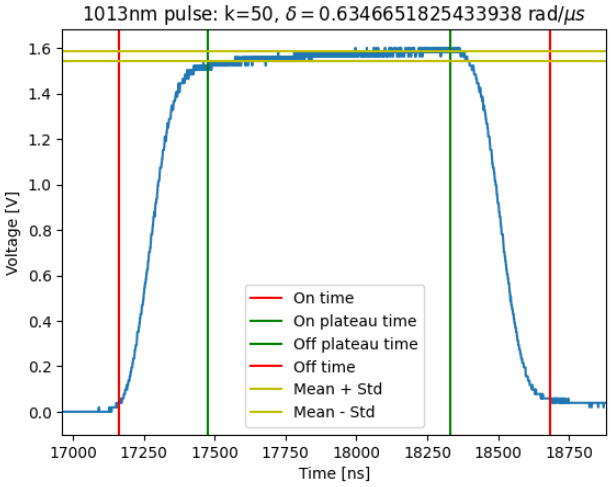

(b) $\delta = 0.63$ rad$/\mu s$

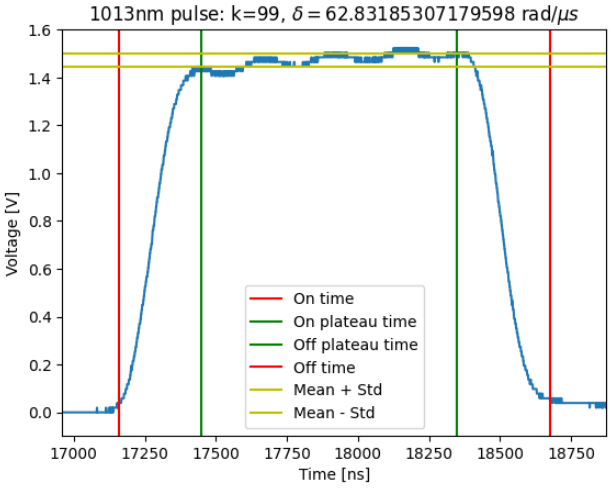

(c) $\delta = 62.83$ rad$/\mu s$

Figure 14: 1013 nm: Square pulses for different input detuning values and equal input amplitude values.

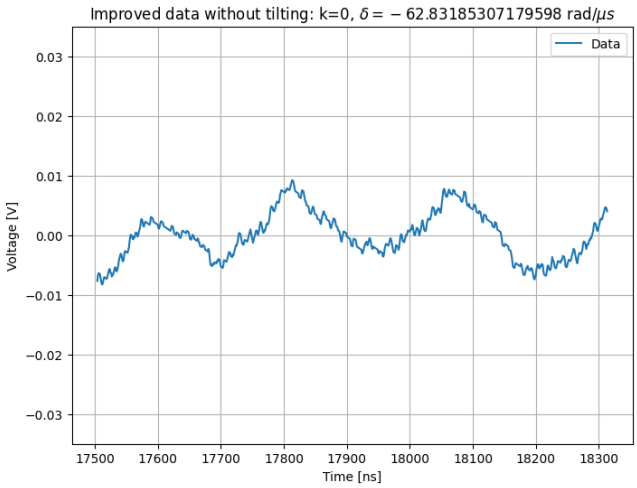

(a) $\delta = 62.83$ rad$/\mu s$

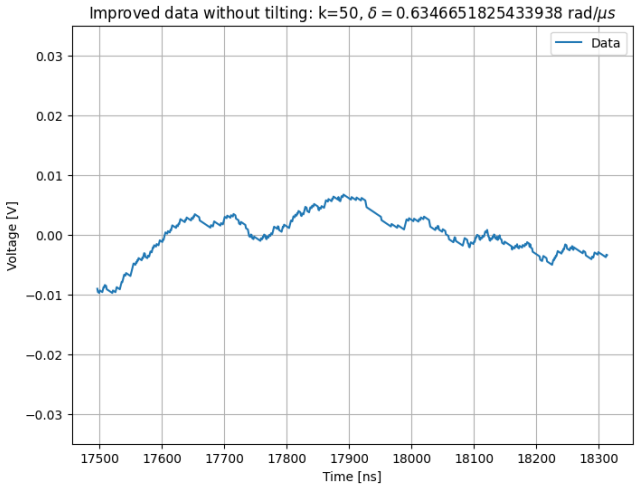

(b) $\delta = 0.63$ rad$/\mu s$

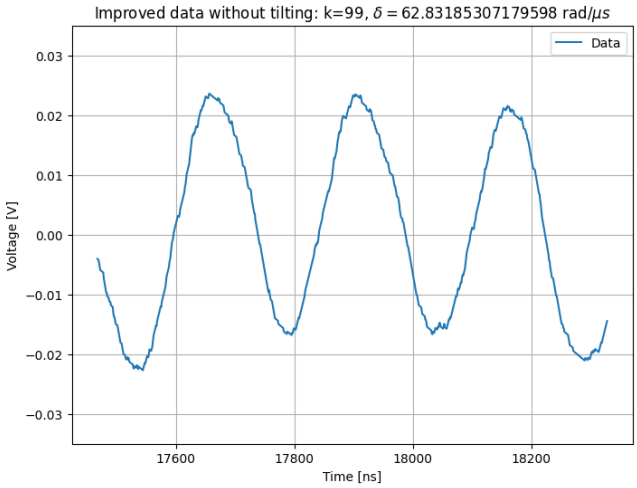

(c) $\delta = 62.83$ rad$/\mu s$

Figure 15: 1013 nm: Plateau oscillations for different input detuning values and equal input amplitude values. The data is filtered and the tilting was removed substracting the linear regression of each plateau.

Double-Pass AOM Theory: A double-pass acousto-optic modulator (AOM) is a device used to control the frequency and intensity of a laser beam. It works by diffracting the laser light using an acoustic wave generated inside a crystal. In a double-pass configuration, the laser beam passes through the AOM twice: the light enters the AOM and is diffracted, what deviates the beam and changes the frequency an amount equal to the frequency of the acoustic wave (ΔF). Later, it is reflected and passes again through the crystal, changing again the frequency of the beam an amount of ΔF [5, 6]. The only possibility that might cause oscillations is an interference between different diffraction modes. However, the system is well controlled with an iris that avoids this.

Possible explanation for the behaviour: The DP AOM detunes the pulse and due to the physical mechanism, there is a quadratic and symmetric reduction of power. The ALS is in charge keeping the light power constant (it operates in saturation mode), while the SP AOM modulates the beam amplitude shape after the ALS has acted.

- Concerning the **oscillations**, maybe the ALS is taking too long to balance the light power because the pulse is too short. Then, we would be measuring the light coming directly form the DP AOM and SP AOM, without fixing the power with the ALS. We suggest that the ALS performs **damped oscillations** to the desired value, but we need a longer pulse to appreciate this.
- Regarding the **tilting** and **voltage variations**, they might be caused by an issue with the ALS, as it is the only device in charge of keeping the voltage constant. The voltage variations must be related to the power loss that the DP AOM causes. As the ALS does not work correctly, we still measure this loss.

  The dependence of the diffraction efficiency (I/I_0) with the radiofrequency detuning (ΔF) behaves as [6]:

$$\frac{I_1}{I_0} = \eta \, \mathrm{sinc}^2\left(\sqrt{\eta + \frac{\Delta\phi^2}{4}}\right) \tag{60}$$

  with

$$\Delta\phi = \frac{\pi\lambda}{v}\frac{\Delta F}{2}\frac{L}{\Lambda_0} \tag{61}$$

	1013 nm
$a_2\ [V/(\mathrm{rad}\ /\mu s)^2]$	$(-1.89 \pm 0.04)\cdot 10^{-5}$
$a_1\ [V/(\mathrm{rad}\ /\mu s)]$	$(-1.28 \pm 0.12)\cdot 10^{-4}$
$a_0\ [V]$	$(1.5582 \pm 0.0007)\cdot 10^{-2}$

Table 1: Fitting parameters for the quadratic dependence of the voltage with the detuning for the 1013 nm laser.

$$\eta = \frac{\pi^2}{2\lambda_0} M_2 \frac{L}{H} P \tag{62}$$

The parameters are:

- I_0, I_1: Intensities of the impinging and outgoing laser sources.
- P_0, P_1: Power of the impinging and outgoing laser sources.
- H, L: height and length of the AOM crystal.
- v, λ, λ_0: Velocity of light in the AOM crystal, wavelength inside the crystal and wavelength of the impinging laser.
- M_2: Acousto-optic figure of merit of the crystal.
- Λ_0: Wavelength of the acoustic wave in the crystal.

This is exactly the behaviour we see since $I_1/I_0 \propto P_1/P_0$ and it can be proved that the expresion 60 can be expanded around $\Delta F = 0$ as

$$\frac{I_1}{I_0} = a_0 + a_2\Delta F^2 + \mathcal{O}(\Delta F^4) \tag{63}$$

that is quadratic with corrections of order $\mathcal{O}(\Delta F^4)$.

Oscillation frequencies dependence with the detuning: I tried to perform a Fourier Transform (FT) over the *plateau data*. The strategy was to take the frequencies with the highest amplitudes and to plot the oscillation frequency with the detuning. However, the pulses were too small and that led to a wrong analysis.

For this reason, I performed a sinusoidal fit for all the 100 pulses as

$$f(x) = \alpha \cdot \sin(\beta x + \gamma) + b \tag{64}$$

with b a parameter to reduce the error when obtaining the angular frequency β.

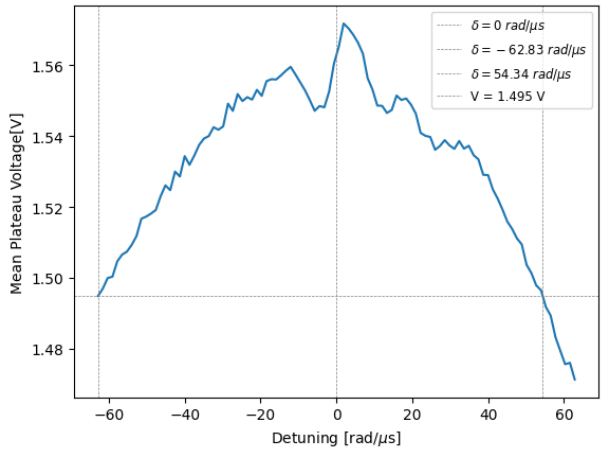

(a) Mean plateau voltage values for each detuning value δ.

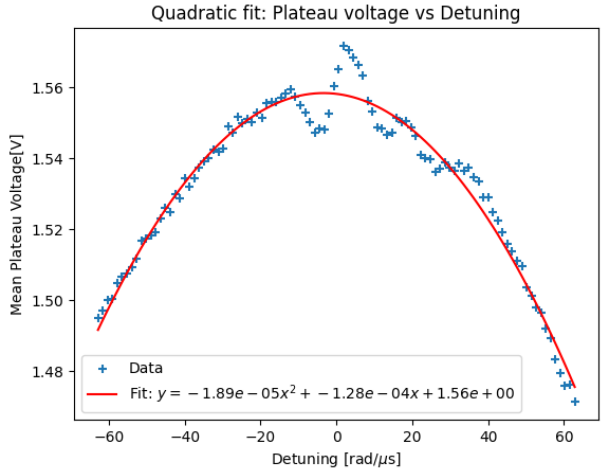

(b) Quadratic fit: Mean plateau voltage values for each detuning value δ. Fitting parameters (as at 65):
$a_2 = (1.89 \pm 0.04) \cdot 10^{-5}$ V/ $(\text{rad}/\mu s)^2$,
$a_1 = (1.28 \pm 0.12) \cdot 10^{-4}$ V/ $(\text{rad}/\mu s)$,
$a_0 = 1.5582 \pm 0.0007$ V.

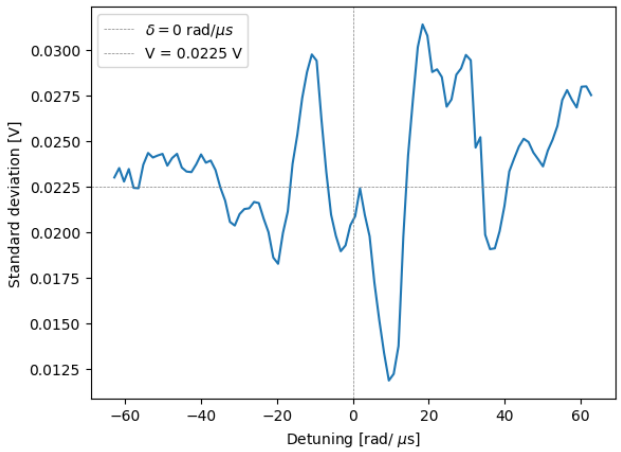

(c) Standard deviation plateau voltage values for each detuning value δ.

Figure 16: 1013 nm: Mean and standard deviation of plateau data for each detuning value δ.

	1013 nm
a_2 $[\text{ns}^{-1}/(\text{rad}/\mu s)^2]$	$(7.71 \pm 0.12) \cdot 10^{-7}$
a_1 $[\text{ns}^{-1}/(\text{rad}/\mu s)]$	$(-4 \pm 4) \cdot 10^{-7}$
a_0 $[\text{ns}^{-1}]$	$(1.157 \pm 0.022) \cdot 10^{-3}$

Table 2: Fitting parameters for the quadratic dependence of the oscillations of the plateau with the detuning for the 1013 nm laser.

In 17a we can see an example of a fit, and in 17b, the frequencies in function of the detuning. The oscillation frequency behaves quadratically and it is symmetric with the detuning respect to $\delta_c \approx 0.28$ rad$/\mu s$, what is negligible compared to the maximum detuning $\delta = 62.83$ rad$/\mu s$ (see table 2). Moreover, $\delta_c = 0$ is in the error range. Then, this anomaly is behaving symmetrically, what was expected, but the quadratic dependence cannot yet be explained.

Possible explanation: I suggest that the oscillation frequency is proportional to the difference of the plateau voltage with the maximum plateau voltage: $f_{osc} \propto |V - V_{max}|$. This is because the ALS performs damped oscillations of the light power until it reaches V_{max} so the oscillations have a higher amplitude and also higher oscillations if the voltage is strongly deviated from V_{max}.

5.4.2 Pulse amplitude analysis

In the figure 18 we see two examples of the square pulses created with the SP AOM (1013 nm) and with the EOM (420 nm). We see that the **EOM rise/fall times are around** $50\% - 25\%$ **of the SP AOM ones**. However, the **EOM pulse is barely constant at the plateau**. This aspect must be fixed to get accurate quantum computing but in the mean time we just want to be able to calibrate the *Quantum Machine* with these pulses as a test.

A quadratic fit was performed over the the plateau voltage and input amplitude data. We see the fitting parameters in the table 3 and the plot in the figure 19, being the fitting function:

$$f(x) = a_2 x^2 + a_1 x + a_0 \tag{65}$$

. The **reason of this dependence** is explained hereunder:

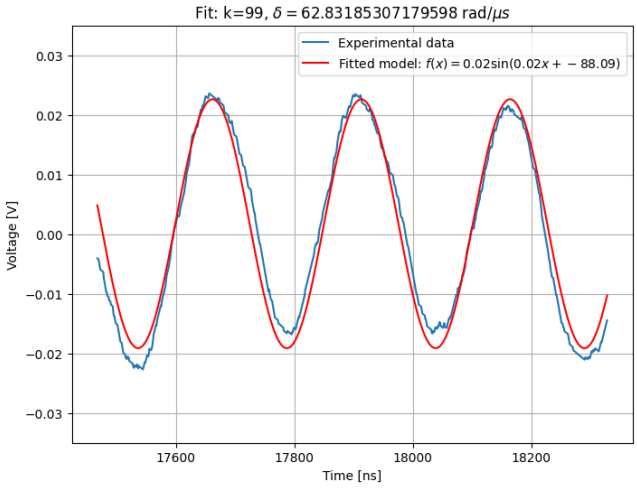

(a) Sinusoidal fit for the pulse with $\delta = 62.83$ rad$/\mu s$ detuning. Fitting parameters (as in 64):
$\alpha = (2.087 \pm 0.014) \cdot 10^{-2}$ V,
$\beta = (2.500 \pm 0.003) \cdot 10^{-2}$ ns^{-1},
$\gamma = -88.1 \pm 0.5$,
$b = (1.75 \pm 0.10) \cdot 10^{-3}$ V.

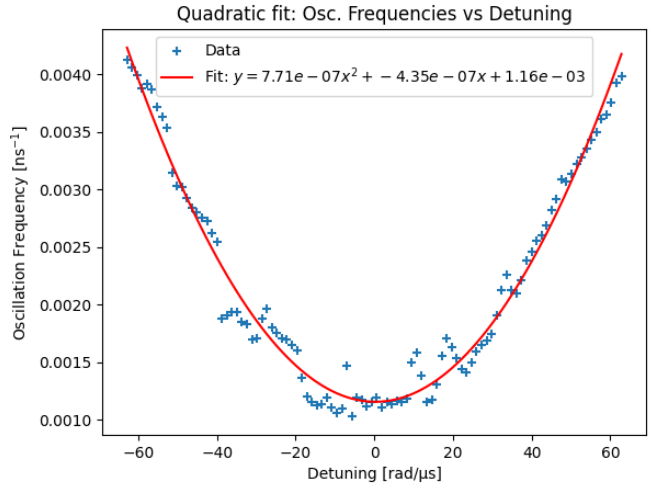

(b) Quadratic fit of the oscillation frequency with the detuning. Fitting parameters (as in 65):
$a_2 = (7.71 \pm 0.12) \cdot 10^{-7}$ ns^{-1}/ (rad$/\mu$s)^2,
$a_1 = (-4 \pm 4) \cdot 10^{-7}$ ns^{-1}/ (rad$/\mu$s),
$a_0 = (1.157 \pm 0.022) \cdot 10^{-3}$ ns^{-1}.

Figure 17: 1013 nm: Example of a sinusoidal fit of the plateau oscillations and a fit showing the relation between the oscillation frequencies and the detuning of each pulse.

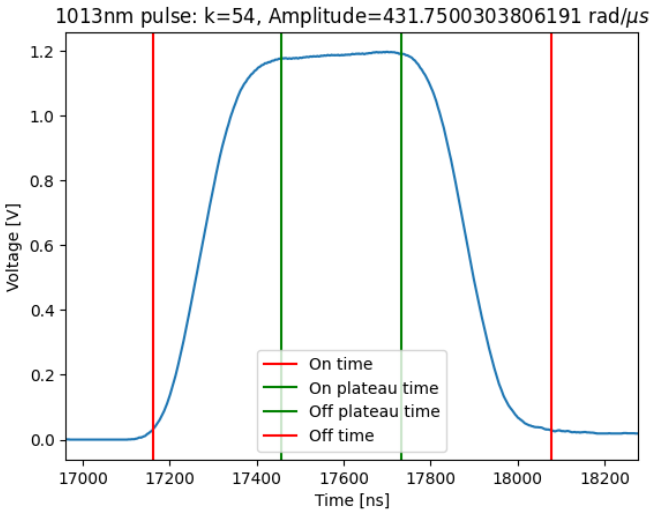

(a) Square laser pulse of 1013 nm created with the SP AOM. The optical power input is 431.75 rad$/\mu s$.

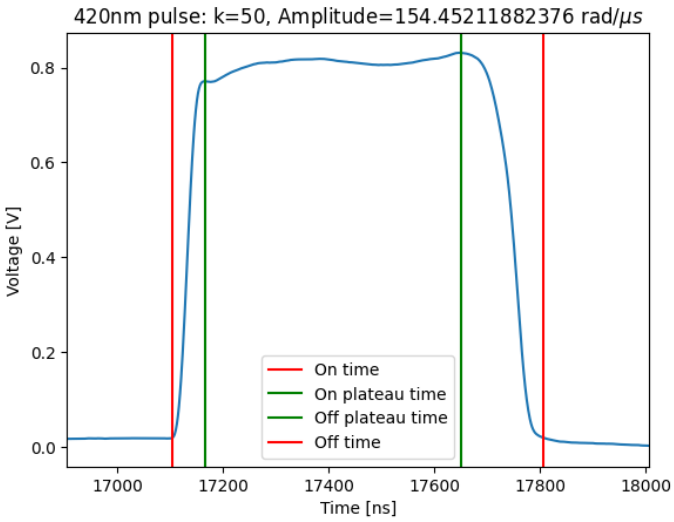

(b) Square laser pulse of 420 nm created with the EOM. The optical power input is 154.45 rad$/\mu s$.

Figure 18: Square pulses with $\delta = 0$ of 1013 nm and 420 nm lasers created with a SP AOM and an EOM respectively.

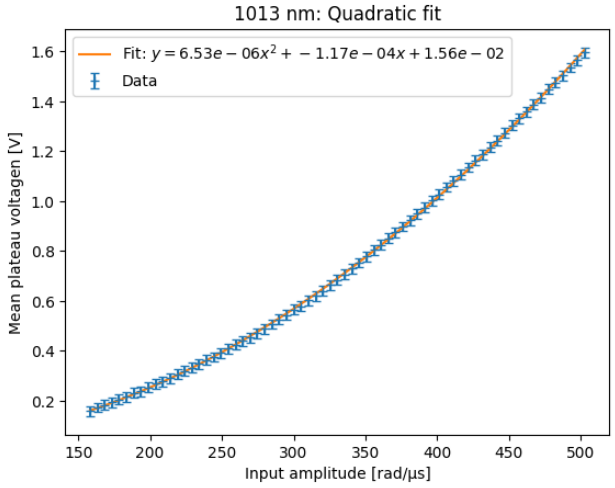

(a) Square laser pulse of 1013 nm created with the SP AOM. The optical power input is 431.75 rad/μs.

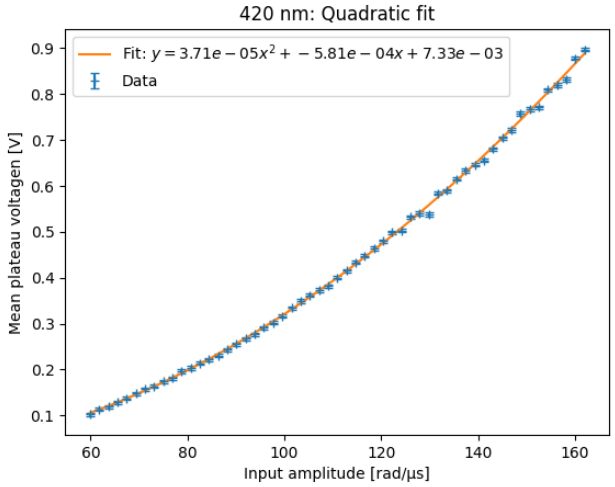

(b) Square laser pulse of 420 nm created with the EOM. The optical power input is 154.45 rad/μs.

Figure 19: Square pulses with $\delta = 0$ of 1013 nm and 420 nm lasers created with a SP AOM and an EOM respectively.

We will assume the simplistic relation:

$$P_\alpha = I_\alpha \cdot A_\alpha = \frac{c\epsilon_0 E_{0,\alpha}^2}{2} \cdot A_\alpha \tag{66}$$

where P_α is the laser power of each beam ($\alpha \in \{0,1\}$), $E_{0,\alpha}$ the respective electric field amplitude, I_α the intensity, and A_α the beam area.

From 9 and 66 we have

$$P = \frac{1}{2}\frac{\varepsilon_0 c\hbar^2}{d_{jk}^2} A \cdot \Omega^2 \tag{67}$$

Moreover, we know that a photodiode, theoretically follows a linear relation between the impinging light power and the recorded voltage:

$$P = k \cdot V \tag{68}$$

and then,

$$I = \frac{k}{A} \cdot V = \alpha V \tag{69}$$

Comparing these relations, finally:

$$V = \frac{1}{2}\frac{\varepsilon_0 c\hbar^2}{d_{jk}^2}\frac{1}{\alpha} \cdot \Omega^2 \tag{70}$$

what gives the quadratic dependence. This is why the engineers in Pasqal programmed the *Quantum Machine* to be calibrated this way.

However, we see that we have non zero a_1, and a_0 parameters, what indicates a possible error in the zero point calibration of the voltage and the input power amplitude value. In any case, it is not that important for the moment.

Finally, if we know the needed dipole operator matrix elements d_{0i} = and d_{i1} **we can calibrate** the *Spectrum* by calculating α_{420}, α_{1013}. Or even better, if we know the calibration of the device, **we can experimentally obtain the dipole operator matrix elements**.

Remark (Rabi Frequency measurement): It is important to highlight that the expression that Pasqal uses to calibrate the *Spectrum* is different from 9. They use the experimental formula 54, that also agrees with the cuadratic behaviour observed.

	1013 nm
$a_2\ [V/(\text{rad}\ /\mu s)^2]$	$(6.53 \pm 0.07) \cdot 10^{-6}$
$a_1\ [V/(\text{rad}\ /\mu s)]$	$(-1.2 \pm 0.4) \cdot 10^{-4}$
$a_0\ [V]$	$(1.6 \pm 0.7) \cdot 10^{-2}$

	420 nm
$a_2\ [V/(\text{rad}\ /\mu s)^2]$	$(3.70 \pm 0.10) \cdot 10^{-5}$
$a_1\ [V/(\text{rad}\ /\mu s)]$	$(-5.8 \pm 2.2) \cdot 10^{-4}$
$a_0\ [V]$	$(0.7 \pm 1.2) \cdot 10^{-2}$

Table 3: Fitting parameters for the quadratic dependence of the voltage with the input power.

6 Conclusions

I comprehended the general map of how Pasqal's QPUs work. This has provided me with valuable insights into the quantum hardware used in quantum computing with cold neutral atoms and how to characterize it. In particular, I specially delved into the laser system operation and the physical mechanisms behind laser cooling, optical tweezers and atom-light interaction.

I was able to understand the theoretical model of a 3-level system of an atom interacting with 2 coherent light sources. This is the model used for quantum computing in Pasqal and I calculated the following results in detail. Starting from the beginning with a dipole interaction Hamiltonian and using the rotating-wave approximation and the adiabatic elimination method, I obtained the equivalent 2-level system, the probability of measuring the atom in each state and the effective Rabi frequency.

I worked on a theoretical model to explain the behaviour of the atom oscillations in an optical trap. The Monte-Carlo simulation reproduced the same behaviour of the atom recapture rate when a laser protocol was applied to measure the oscillation frequency.

I learned to define pulses sequences with the Rydberg lasers and I created new ones to characterize the square pulses. To achieve this, I learned new techniques to process noisy signals.

I calibrated the *Spectrum* device by finding a quadratic relation between the voltage of the square pulse and the input Rabi frequency received by the laser. This was as expected: it was programmed this way since, theoretically, the Rabi frequency of an atom interacting with a laser source and the light power have this dependence.

Finally, I focused on the anomalies that the team and I found in the light square pulse signals. There were oscillations at the plateau whose frequency changed quadratically with the detuning applied. The mean voltage at the plateau also changed quadratically with the detuning while they should be constant. After analyzing the quantum hardware that controls the lasers and gaining theoretical insight into double-pass acousto-optic modulators (DP AOMs), we concluded that the issue was caused by a malfunction of the ALS amplifier. However, this must still be discussed.

References

[1] Lucas Beguin
Measurement of the van der Waals interaction between two Rydberg atoms.
Other [cond-mat.other]
Institut d'Optique Graduate School, 2013.
English. NNT : 2013IOTA0004.
pastel-00936072

[2] Benoît Darquié
Manipulation d'atomes dans des pièges dispolaires microscopiques et émission côntrolée de photons par un atome unique
Physique Atomique [physics.atom-ph].
Université Paris Sud - Paris XI, 2005.
Français. NNT : ff. fftel-00011604

[3] C. Tuchendler, A. M. Lance, A. Browaeys, Y. R. P. Sortais and P. Grangier
Energy distribution and cooling of a single atom in an optical tweezer
PACS numbers: 37.10.Jk, 42.50.Ct, 03.67.-a

[4] Rui HAN, Hui Khoon NG and Berthold-Georg ENGLERT;
Raman transitions without adiabatic elimination: a simple and accurate treatment
http://dx.doi.org/10.1080/09500340.2013.770573
Journal of Modern Optics, Vol. 60, No. 4, Pp. 255-265, Feb. 2013
Publisher: Informa UK Limited

[5] Kogelnik, H.;
Theory of Dielectric Waveguides
In: Tamir, T;
Theory of Integrated Optics
https://doi.org/10.1007/978-3-662-43208-2_2
Topics in Applied Physics, vol 7
Springer, Berlin, Heidelberg

[6] AA OPTO-ELECTRONIC;
Acousto-optic Theory. Application Notes.
https://pegasus-optik.de/wp-content/uploads/2019/06/AO-Theorie.pdf